Enhancing low-temperature activity and durability of Pd-based diesel oxidation catalysts using ZrO₂ supports☆

Mi-Young Kim [a,1], Eleni A. Kyriakidou [a], Jae-Soon Choi [a,*], Todd J. Toops [a], Andrew J. Binder [a], Cyril Thomas [b,c], James E. Parks II [a], Viviane Schwartz [d], Jihua Chen [d], Dale K. Hensley [d]

[a] Fuels, Engines, and Emissions Research Center, Oak Ridge National Laboratory, Oak Ridge, TN, USA
[b] Sorbonne Universités, UPMC Univ Paris 06, UMR 7197, Laboratoire de Réactivité de Surface, 4 Place Jussieu, Case 178, F-75252 Paris, France
[c] CNRS, UMR 7197, Laboratoire de Réactivité de Surface, 4 Place Jussieu, Case 178, F-75252 Paris, France
[d] Center for Nanophase Materials Sciences, Oak Ridge National Laboratory, Oak Ridge, TN, USA

ARTICLE INFO

ABSTRACT

We investigated the impact of ZrO₂ on the performance of palladium-based oxidation catalysts with respect to low-temperature activity, hydrothermal stability, and sulfur tolerance. Pd supported on ZrO₂ and SiO₂ were synthesized for a comparative study. Additionally, in an attempt to maximize the ZrO₂ surface area and improve sulfur tolerance, a Pd support with ZrO₂-dispersed onto SiO₂ was studied. The physicochemical properties of the catalysts were examined using ICP, N₂ sorption, XRD, SEM, TEM, and NH₃-, CO₂-, and NOₓ-TPD. The activity of the Pd catalysts were measured from 60 to 600 °C in a flow of 4000 ppm CO, 500 ppm NO, 1000 ppm C₃H₆, 4% O₂, 5% H₂O, and Ar balance. The Pd catalysts were evaluated in fresh, sulfated, and hydrothermally aged states. Overall, the ZrO₂-containing catalysts showed considerably higher CO and C₃H₆ oxidation activity than Pd/SiO₂ under the reaction conditions studied. The good performance of ZrO₂-containing catalysts appeared to be due in part to high Pd dispersion resulting from strong Pd and support interaction. Another beneficial effect of strong interaction between Pd and ZrO₂ was manifested as a greater hydrothermal stability with good oxidation activity even after aging at 800 and 900 °C for 16 h. In contrast, Pd/SiO₂ suffered significant performance loss due to Pd particle coarsening. Although the Pd/ZrO₂-SiO₂ catalyst was not more active than Pd/ZrO₂, improved tolerance to sulfur was realized. Unlike the bulk ZrO₂ support, the ZrO₂-incorporated SiO₂ presented only weak basicity leading to a superior sulfur tolerance of Pd/ZrO₂-SiO₂. These results confirmed the potential of developing Pd-based oxidation catalysts with enhanced low-temperature activity and durability using ZrO₂-SiO₂ supports. Controlling morphology and accessible area of the dispersed ZrO₂ layer appeared critical to further maximize the catalytic performance.

© 2016 Elsevier B.V. All rights reserved.

1. Introduction

With ever tightening automotive emission standards, the role of oxidation catalysts becomes increasingly more important to remove CO and unburned hydrocarbons (HCs) from the engine exhaust gas as well as to enhance the performance of downstream NOₓ control catalysts [1–3]. Moreover, as the efficiency of internal combustion engines is required to improve in response to US EPA's Corporate Average Fuel Economy (CAFE) mandates, the average exhaust gas temperature decreases making it more and more challenging to maintain high performance of aftertreatment catalysts. To comply with the future emission and fuel economy regulations, automotive catalysts should therefore achieve catalyst light-off (50% or higher conversion) at temperatures significantly lower than the current state of the art.

Despite recent progress made in the low-temperature catalyst development with novel formulations such as Au and Ag nanoparticles supported on metal oxides [4–7], critical challenges remain in implementing these novel materials into practice. For instance, new catalysts should be able to maintain high activity under harsh real automotive environments with good thermal stability and resistance to poisons [8,9]. Due to relatively good stability and activity, Pt and/or Pd supported on CeO_2-ZrO_2 added Al_2O_3 supports have been widely used as commercial oxidation catalysts [1,10]. The high affinity of Al_2O_3 toward sulfur, however, can lead to the formation of $Al_2(SO_4)_3$ with resultant performance degradation [11]. In addition, repeated high-temperature desulfation can lead to gradual sintering of metal components with resultant permanent activity loss. To further enhance the low-temperature activity and stability of Pt and Pd catalysts, recent research efforts have been devoted to developing novel approaches including the use of FeO_x as a support [12–14] and the encapsulation in core-shell nanostructures [15,16].

We have recently reported that Pt particles supported on ZrO_2-modifed SiO_2 were excellent CO oxidation catalysts with promising low-temperature activity, hydrothermal stability, and sulfur tolerance [17]. Covering SiO_2 surfaces with ZrO_2 via sol-gel method before Pt impregnation led to good dispersion and hydrothermal stability of Pt particles due to strong interaction between Pt and ZrO_2 phases. Furthermore, ZrO_2 incorporation generated surface acidity but negligible basicity, which explained the relatively low and weak sulfur uptake observed on Pt/ZrO_2-SiO_2. We also revealed that ZrO_2 increased the oxygen affinity of Pt leading to good catalytic activity of Pt/ZrO_2-SiO_2 in CO oxidation. In the present study, we extended this ZrO_2-incorporated SiO_2 support concept to Pd, a commonly-employed automotive catalyst that is traditionally less expensive than Pt by a factor of 2–3. For comparison, the catalytic properties of Pd/ZrO_2 and Pd/SiO_2 were studied. This paper will show that, as in the case of Pt, ZrO_2 incorporation on SiO_2 has positive effects on Pd as well with good metal dispersion, hydrothermal stability, sulfur tolerance, and CO and C_3H_6 oxidation activity. Directions for future research will be discussed to facilitate the development of strategies to maximize the potential of ZrO_2 supports.

2. Experimental

2.1. Preparation of Pd catalysts

Amorphous silica gel (Davisil Grade 635, pore size 60 Å, 60–100 mesh, Sigma-Aldrich) was used as a support for the preparation of Pd catalysts. ZrO_2 was incorporated on the silica surface following the procedure described in previous papers [17,18]. SiO_2 was first dehydrated with anhydrous ethanol (200 proof, ACS reagent, ≥99.5%, Sigma-Aldrich) and reacted at 80 °C for 3 h with zirconium(IV) n-propoxide (70% w/w in n-propanol, Alfa Aesar) dissolved in ethanol. The ratio between SiO_2, Zr precursor solution, and ethanol was 1: 2: 16 on a weight basis. The amount of Zr precursor molecules in the mixture corresponded to an average silanol concentration on the SiO_2 surface assumed to be 7.5 μmol/m^2 based on [19]. Since more than 1 silanol group would have reacted with a Zr precursor molecule during the sol-gel process, unreacted Zr precursor molecules were removed through ethanol washing. Subsequently, the filtrates were dried at 100 °C overnight and calcined at 500 °C for 2 h. The resulting ZrO_2-SiO_2 support was impregnated with a palladium (II) nitrate solution (12~16 w/w, Alfa Aesar) by incipient wetness method to obtain a 1 wt% Pd loading. After the impregnation, the catalyst was dried at 100 °C in air and reduced in a flow of 10% H_2 in Ar at 500 °C for 2 h. The as-prepared catalyst was named as Pd/ZrO_2-SiO_2. For comparison, Pd catalysts supported on bare SiO_2 (Pd/SiO_2) and ZrO_2 (Pd/ZrO_2; ZrO_2 from

Saint-Gobain) were also prepared by incipient wetness method (1 wt% loading).

2.2. Characterization

The Zr and Pd contents of the prepared catalysts were determined using Inductively Coupled Plasma-Atomic Emission Spectrometry (ICP-AES; Optima 4300 DV, Perkin-Elmer, USA). The surface area and porosity of catalysts were determined using an automatic volumetric adsorption apparatus (Autosorb-1, Quantachrome, USA). The samples were evacuated at 200 °C for 2 h prior to exposure to nitrogen gas. Surface areas were calculated using the Brunauer-Emmett-Teller (BET) equation and the pore volumes and average pore sizes were determined using the Barrett-Joyner-Halenda (BJH) method.

In powder XRD, the catalysts were ground into fine powder and placed on a zero background carbon plate of approximately 3.8 cm in diameter. The X-ray diffraction patterns of catalysts were recorded on a powder X-ray Diffractometer (XRD; X'Pert PRO, PANalytical, The Netherlands) operated at 45 kV and 40 mA using CuKα radiation ($K\alpha$ = 0.154178 nm) over a 2θ angle of 5–50 in a scan mode of 0.02° in 2s.

A Transmission Electron Microscope (TEM; LIBRA-120, Carl Zeiss, Germany) equipped with a LaB$_6$ filament was employed to examine the Pd dispersion. The acceleration voltage was 120 kV. The TEM samples were prepared by dropping ethanol suspension of Pd catalysts on a copper grid. The particle size of Pd was estimated from the digitized TEM image using analysis software (ImageJ, NIH, USA). The Scanning Electron Microscope (SEM; Merlin, Carl Zeiss, Germany) analyses were performed to examine the morphology of Pd catalysts, operating at an accelerating voltage of 30 kV. Elemental mapping analyses were also performed using Energy Dispersive X-ray Spectroscopy (EDS; Bruker Nano Gmbh with a XFlash 5030 detector, Germany) attached to the SEM.

NH_3- and CO_2-Temperature-Programmed Desorption (TPD) experiments were carried out with a flow reactor system. For each TPD experiment, 0.1 g of catalyst was placed between two quartz wool plugs in a U-shaped quartz tube (8 mm I.D.) and pretreated at 600 °C for 0.5 h in an Ar flow. After cooling to 100 °C, the catalyst was exposed to a flow of 2500 ppm NH_3 in Ar for 1 h, then to an Ar flow for 1 h. Desorption was carried out in an Ar flow from 100 to 600 °C with a temperature ramping rate of 10 °C/min. The total flow rate was 50 mL/min (STP) for all the steps. The procedure for the CO_2-TPD experiments was identical except that the adsorption was done in a flow of 1% CO_2 in Ar at 50 °C followed by a 1 h purge with the total flow rate of 100 mL/min (STP). Gas composition was continuously analyzed by a quadrupole mass spectrometer (RGA100, SRS, USA). The m/z values monitored were 15 for NH_3 and 44 for CO_2.

NO_x-TPD experiments were performed in a U-shaped quartz reactor (15 mm I.D.). The details were introduced in [20,21]. The catalysts were pretreated in a 20% O_2/He flow at 500 °C for 2 h with a flow rate of 100 mL/min. After cooling to room temperature, the catalysts were exposed to the adsorption mixture which consisted of 400 ppm NO and 8% O_2 in He. NO_x-TPD experiments were performed from room temperature to 560 °C at a heating rate of 3 °C/min under a mixture of 8% O_2 in He with a total flow rate of 230 mL/min (STP). The gas composition was continuously monitored at reactor outlet by a chemiluminescence NO_x analyzer (42C-HT, Thermo Environmental Instruments). The NO_x-TPD profiles were corrected for the weight loss due to dehydration of the samples.

2.3. Evaluation of catalytic performance in oxidation reactions

The catalytic performance of the prepared catalysts was evaluated for CO and C_3H_6 oxidation activity under simulated diesel

exhaust conditions. A flow reactor equipped with a quadrupole mass spectrometer (RGA100, SRS, USA) was employed. As previously described in [22], it has two gas banks controlled by a 4-way valve and a bypass line for flow equilibration and calibration. The gas flow rates were adjusted with mass flow controllers and the furnace temperature was controlled by a PID temperature controller. For each reactor run, 0.1 g of Pd catalyst was positioned between two plugs of quartz wool in a U-shaped quartz tube. Prior to the experiments, the catalysts were pretreated in an Ar flow at 600 °C for 1 h. The reactant gas mixture consisting of 4000 ppm CO, 1000 ppm C_3H_6, 500 ppm NO, 4% O_2, 5% H_2O, and Ar balance was fed into the reactor at a total flow rate of 200 mL/min (STP). The performance was evaluated by continuously increasing the reaction temperature from 60 to 600 °C at 5 °C/min. The effluent gas composition was analyzed with the mass spectrometer. The monitored m/z ratios were 26 for C_3H_6, 28 for CO, and 44 for CO_2. To obtain CO concentration values, the contribution from CO_2 fragmentation at m/z 28 was taken into account. Several consecutive oxidation runs were performed for each catalyst in the order of fresh, sulfated, desulfated, and hydrothermally aged states.

Following the fresh-state performance evaluation, the catalyst was sulfated at 400 °C in 50 ppm SO_2, 5% H_2O, 4% O_2, and Ar balance for 3 h. After sulfation, all weakly bound sulfur species were removed by shutting off the SO_2 flow and purging at 400 °C for 30 min before another reactor evaluation. The sulfur exposed catalysts were then desulfated consecutively at 600, 700 and 800 °C (temperature ramp from 400 °C at 5 °C/min) for 1 h in a rich phase gas mixture including 1% H_2, 5% H_2O, and Ar balance. After each desulfation step and prior to further evaluation, the samples were pretreated at 600 °C in 4% O_2, 5% H_2O, and Ar balance for 1 h. For sulfur analysis, a fluorescent SO_2 analyzer (100 A UV fluorescence SO_2 analyzer, Teledyne API, San Diego, CA, USA) was used. A second reactor loaded with an oxidation Pt/SiO_2 catalyst was placed downstream of the main reactor to oxidize any H_2S to SO_2, since the sulfur analyzer detected only SO_2 [23]; a stream of O_2 was introduced after the main reactor, but before the second reactor to allow this oxidation. Assuming a thermodynamic equilibrium between SO_2 and SO_3 was reached over the downstream reactor operated at 700 °C, the total sulfur concentration could be determined (i.e., $SO_2 + SO_3 + H_2S$).

Following the sulfation/desulfation study, the catalysts were hydrothermally aged at 800 °C for 16 h in a flow of 10% O_2, 5% H_2O, and Ar balance. After a performance evaluation run, the catalysts were further aged at 900 °C for 16 h in the same flow used for the 800 °C aging.

3. Results and discussion

3.1. Catalyst characterization

Table 1 lists the chemical composition and some physical properties of Pd catalysts. The target Pd loading was 1 wt% and actual values determined by ICP were ca. 1.1 wt%. The surface area of Pd/ZrO_2, Pd/SiO_2, and Pd/ZrO_2-SiO_2 was, respectively, 93, 447, and 404 m^2/g at the fresh state and 24, 301, and 325 m^2/g after the aging at 800 °C for 16 h. The fact that the surface area of Pd/ZrO_2-SiO_2 was almost identical to that of Pd/SiO_2 indicates that thin layers and/or small particles of ZrO_2 were formed on SiO_2 surfaces. The slight decrease in surface area reported per g of sample is expected since ZrO_2 is heavier than SiO_2. The surface area for Pd/ZrO_2-SiO_2 would be 483 m^2/g_{SiO_2} compared to 447 m^2/g for SiO_2, suggesting that ZrO_2 also contributed in developing surface area and that it is not just a coverage of SiO_2. The surface area and pore volume of all Pd catalysts decreased after hydrothermal aging suggesting significant structural changes such as crystallization, particle growth, pore
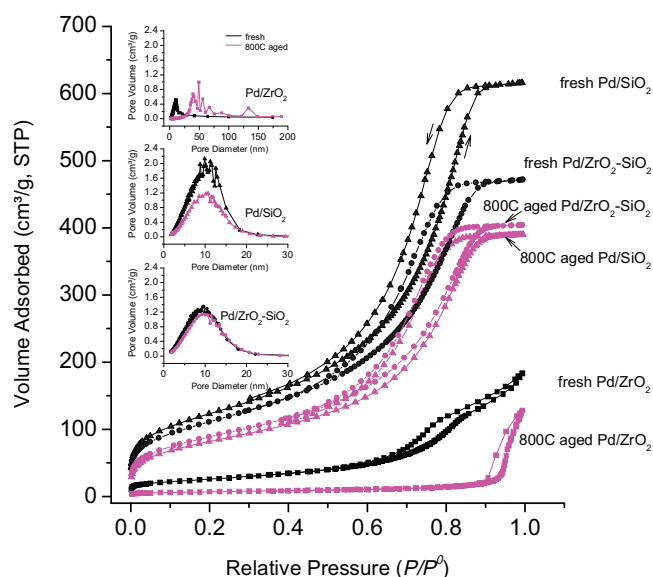

Fig. 1. Nitrogen adsorption and desorption isotherms of Pd/ZrO_2, Pd/SiO_2, and Pd/ZrO_2-SiO_2 in fresh and hydrothermally aged states. The inset figures present BJH pore size distributions for Pd catalysts as determined from the nitrogen adsorption curves.

blocking and pore wall collapse. Nevertheless, a ZrO_2-induced stabilization of the SiO_2 surface area can be seen in the Pd/ZrO_2-SiO_2 hydrothermally-aged data. Indeed, the surface area and porosity loss for the Pd/ZrO_2-SiO_2 were smaller than those of Pd/SiO_2 and Pt/ZrO_2. These results indicate that the addition of ZrO_2 to SiO_2 can lead to a more stable support compared to bulk SiO_2 or ZrO_2.

The N_2 adsorption-desorption isotherms for Pd catalysts are represented in Fig. 1. The Pd catalysts supported on SiO_2 and ZrO_2-SiO_2 exhibited typical Type IV isotherms [24] with a hysteresis loop associated with capillary condensation in mesopores at both fresh and aged state. The Pd/ZrO_2 in fresh state also showed a similar behavior. By contrast, the aged Pd/ZrO_2 showed N_2 isotherms with a negligible "knee" point and presented a wide pore size distribution. The lack of knee point represents weak adsorbate-adsorbent interaction resulting in low BET surface area. This indicates that physical properties of Pd/ZrO_2 were more severely affected by hydrothermal aging than those of Pd/SiO_2 and Pd/ZrO_2-SiO_2.

X-ray diffraction patterns were recorded for each sample to investigate both crystallographic phases present and their crystallinity (Fig. 2). Pd/ZrO_2 sample showed diffraction peaks corresponding to a monoclinic ZrO_2 at 17.4, 24.0, 28.2, 31.4, 34.1, 35.3, 40.7, 44.8, 45.5 and 48.9° (ICDD# 00-024-1165). The peaks grew with increasing the aging temperature indicating ZrO_2 particle aggregation which is consistent with the N_2 sorption data. The relatively weak thermal stability of the monoclinic ZrO_2 phases is well-known and could be a significant challenge to overcome for very demanding automotive applications [25]. No significant diffraction peaks associated with Pd or PdO were observed. In general, the peaks related to cubic Pd particles should appear at 2θ of 39.0, 40.1 and 46.6° (ICDD# 01-087-0637 and ICDD# 00-046-1043), while the (101) plane of tetragonal PdO is found at 2θ of 33.8° (ICDD# 04-002-4417) (see the two areas marked with red boxes in Fig. 2). The absence of Pd peaks on Pd/ZrO_2 suggests that Pd was well dispersed due to strong interaction between the metal and support. Considering the large impact of aging on the ZrO_2 support this lack of impact on the Pd particles are surprising. In contrast, Pd/SiO_2 exhibited peaks attributable to Pd and PdO particles after aging at 900 °C; the broad peak at 2θ of 22° corresponded to amorphous SiO_2 structure. The fresh Pd/ZrO_2-SiO_2 presented a small peak of PdO at 33.8°. The PdO peak became sharper with aging at 800 °C of

Table 1
Chemical composition and physical properties of Pd catalysts.

Samples	Composition (wt%)[a]		Surface area	Pore volume	Average pore	Pd particle size
	Pd	Zr	(m^2/g)[b]	(cm^3/g)[b]	size (nm)[b]	(nm)[c]
Fresh Pd/ZrO$_2$	1.13	n.d.	93	0.278	9.8	n.d.
Aged Pd/ZrO$_2$[d]	n.d.	n.d.	24	0.196	32.5	1.1 ± 0.3
Fresh Pd/SiO$_2$	1.13	n.d.	447	0.903	7.1	2.4 ± 1.1
Aged Pd/SiO$_2$[d]	n.d.	n.d.	301	0.562	7.0	4.1 ± 1.8
Fresh Pd/ZrO$_2$-SiO$_2$	1.14	12.1	404	0.680	6.3	3.6 ± 2.0
Aged Pd/ZrO$_2$-SiO$_2$[d]	n.d.	n.d.	325	0.578	6.7	1.9 ± 1.0

[a] Measured by ICP-AES.
[b] Measured at liquid nitrogen temperature.
[c] Calculated from TEM images; number of Pd particles measured: 34–184.
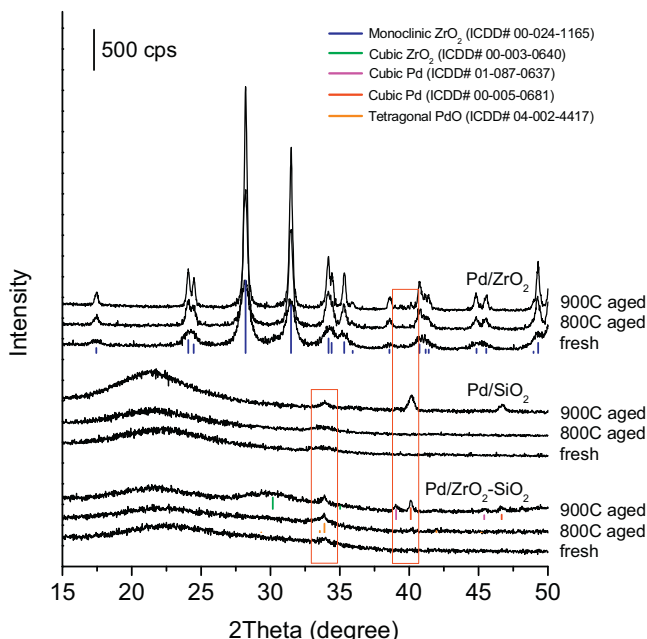[d] Aged at 800 °C for 16 h.

Fig. 2. XRD patterns of Pd/ZrO$_2$, Pd/SiO$_2$, and Pd/ZrO$_2$-SiO$_2$ in fresh and hydrothermally aged states.

Pd/ZrO$_2$-SiO$_2$. After the aging at 900 °C, Pd metal-attributable peaks also appeared; the broad peak at 30° is attributable to a cubic ZrO$_2$ phase (ICDD# 00-003-0640). The smaller Pd peaks on Pd/ZrO$_2$-SiO$_2$ than Pd/SiO$_2$ on the aged state at 900 °C suggests that the addition of ZrO$_2$ on SiO$_2$ increased Pd-support interactions.

Transmission electron microscopy images and particle size distributions in Fig. 3 show clear differences in the size of Pd particles among samples. Average Pd particle sizes are listed in Table 1. No Pd particles were observed by TEM on Pd/ZrO$_2$ in the fresh state due to a very high Pd dispersion. After aging at 800 °C, the Pd particles with the average size of 1.1 nm were detected. This means that although the hydrothermal aging induced a considerable decrease in surface area, the ZrO$_2$ support was still able to maintain a high Pd dispersion. In the case of Pd/SiO$_2$ and Pd/ZrO$_2$-SiO$_2$, Pd particles in the range from 1 nm to 12 nm were observed. Contrary to the previously published results on Pt catalysts [17], the fresh Pd/SiO$_2$ had smaller Pd particles than the fresh Pd/ZrO$_2$-SiO$_2$ with an average value of 2.4 nm. Pd particles on SiO$_2$ were, however, more prone to sintering during hydrothermal aging at 800 °C. In fact, the average Pd particle size on ZrO$_2$-SiO$_2$ decreased with aging at 800 °C. We conjecture that a portion of Pd atoms initially deposited on exposed SiO$_2$ surfaces with weaker metal-support interaction migrated onto ZrO$_2$ surfaces during the aging step and stabilized as smaller particles on ZrO$_2$ surfaces of the ZrO$_2$-SiO$_2$ support achieving a higher Pd

dispersion after the aging. Further research is, however, needed to support this hypothesis and more clearly explain this unexpected behavior for instance using H$_2$ chemisorption.

Fig. 4 shows SEM images and EDX Pd maps of the catalysts aged at 900 °C. Pd particles were still well-dispersed on Pd/ZrO$_2$, while large aggregates were observed on both Pd/SiO$_2$ and Pd/ZrO$_2$-SiO$_2$ catalysts. The large aggregates observed on Pd/ZrO$_2$-SiO$_2$ were more likely concentrated on exposed SiO$_2$ surfaces (i.e., not coated by ZrO$_2$) as those aggregate-containing regions presented lower Zr/Si ratio than other regions with fewer Pd aggregates (data not shown). This is consistent with the above TEM data.

The extent of SiO$_2$ surface coverage by ZrO$_2$ was estimated using NO$_x$-TPD to better understand the effectiveness of the sol-gel method employed as well as the observed performance trends. It has previously been demonstrated by Thomas et al. that NO$_x$ chemisorption selectively occurs on ZrO$_2$ and not on SiO$_2$ or tungstates [20,21], which makes NO$_x$-TPD a reliable tool to estimate the accessible zirconia surface area of a variety of ZrO$_2$-containing materials [20,21]. The NO$_x$-TPD profiles of Pd/ZrO$_2$ and Pd/ZrO$_2$-SiO$_2$ are shown in Fig. 5 and the corresponding data are summarized in Table 2. The NO$_x$-TPD profiles obtained on the fresh ZrO$_2$ support closely resembled to those found earlier [21] showing well-resolved low and high temperature (LT: 85 °C and HT: 420 °C) NO$_x$ desorption peaks (not shown). As already noticed recently in the case of the introduction of Rh on tungstated Ce$_{0.68}$Zr$_{0.32}$O$_2$ materials [26], the introduction of Pd significantly decreased the resolution of the LT and HT desorption peaks on fresh Pd/ZrO$_2$ (Fig. 5), with the desorption of NO$_x$ species at intermediate temperatures (120–250 °C) and a shift of the HT peak to slightly lower temperature (400 °C). In contrast, the introduction of Pd on ZrO$_2$-SiO$_2$ did not decrease the resolution of the LT and HT desorption peaks as much as in the case of fresh Pd/ZrO$_2$ (Fig. 5) suggesting that Pd would have been deposited on exposed SiO$_2$ surfaces (i.e., not coated by ZrO$_2$) as well in agreement with the TEM, SEM and EDX results. It is remarkable that NO$_x$ desorption behavior on ZrO$_2$-SiO$_2$ was quite different from that of bulk ZrO$_2$ support. For example, the LT and HT peaks of Pd/ZrO$_2$ were observed at 90 °C and 400 °C, while those of Pd/ZrO$_2$-SiO$_2$ appeared at 85 °C and 325 °C in the fresh state. Furthermore, while the intensity of LT peak was lower than that of HT peak on the fresh Pd/ZrO$_2$, the intensity of LT peak was higher than that of HT peak on the fresh Pd/ZrO$_2$-SiO$_2$. We can thus conclude that Pd/ZrO$_2$ had overall more stable NO$_x$ species adsorbed on the surface than Pd/ZrO$_2$-SiO$_2$ presumably due to stronger surface basicity as will be supported later by CO$_2$-TPD results. The NO$_x$ uptake of the fresh Pd/ZrO$_2$ and Pd/ZrO$_2$-SiO$_2$ was 495 and 327 μmol/g, respectively. These correspond to an accessible ZrO$_2$ surface area of 83 m^2/g for Pd/ZrO$_2$ and 54 m^2/g for Pd/ZrO$_2$-SiO$_2$. By comparing the BET surface area of Pd/ZrO$_2$-SiO$_2$ with the accessible ZrO$_2$ surface area determined by NO$_x$ TPD, it is possible to estimate that at most about 13% of SiO$_2$ surface was covered by ZrO$_2$. Considering that the Zr loading of 12.1 wt% achieved
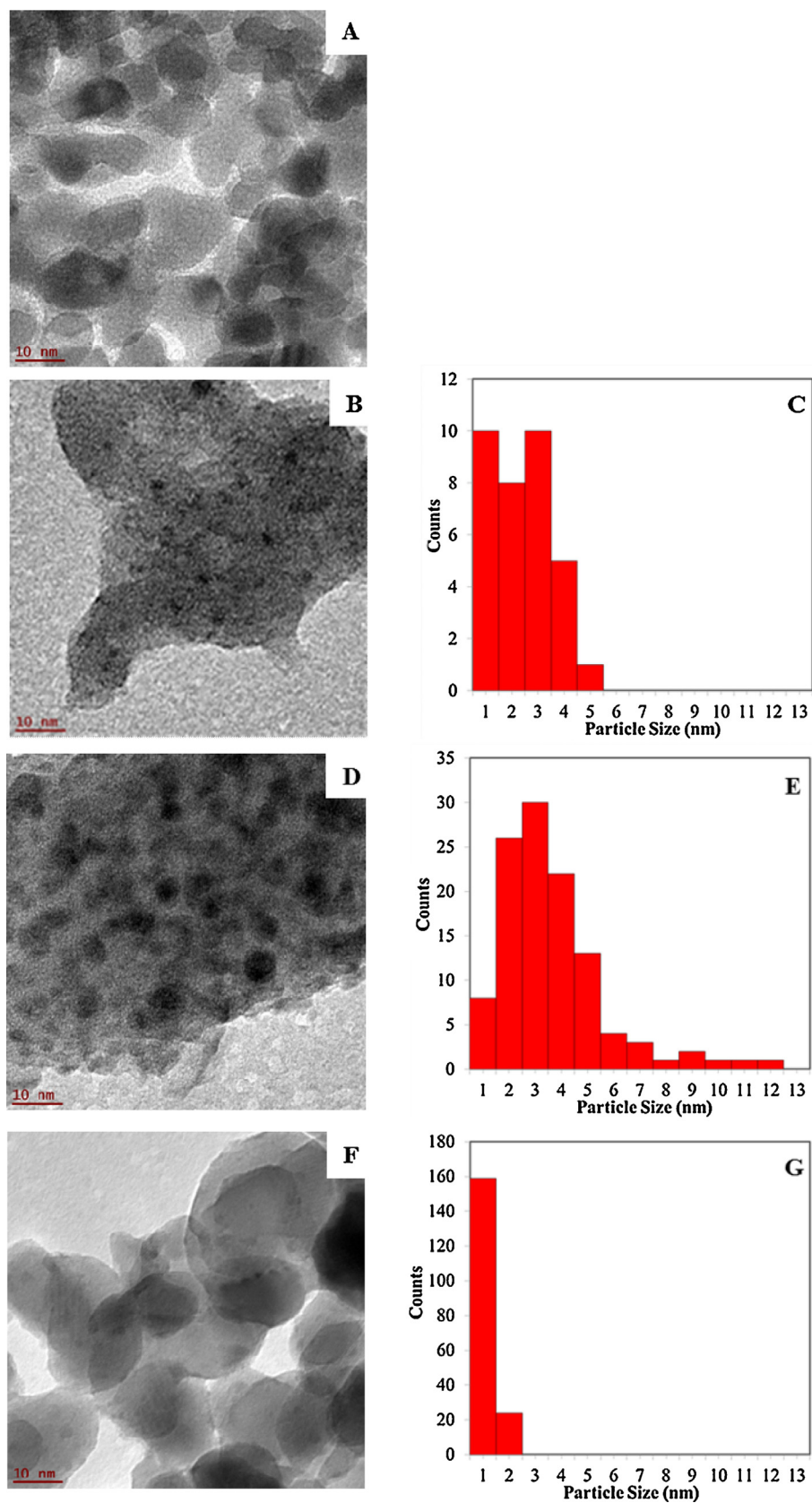
Fig. 3. TEM micrographs and particle size distributions of fresh Pd/ZrO_2 (A), fresh Pd/SiO_2, (B, C), fresh Pd/ZrO_2-SiO_2 (D, E), 800 °C-aged Pd/ZrO_2 (F, G), 800 °C-aged Pd/SiO_2 (H, I) and 800 °C-aged Pd/ZrO_2-SiO_2 (J, K).
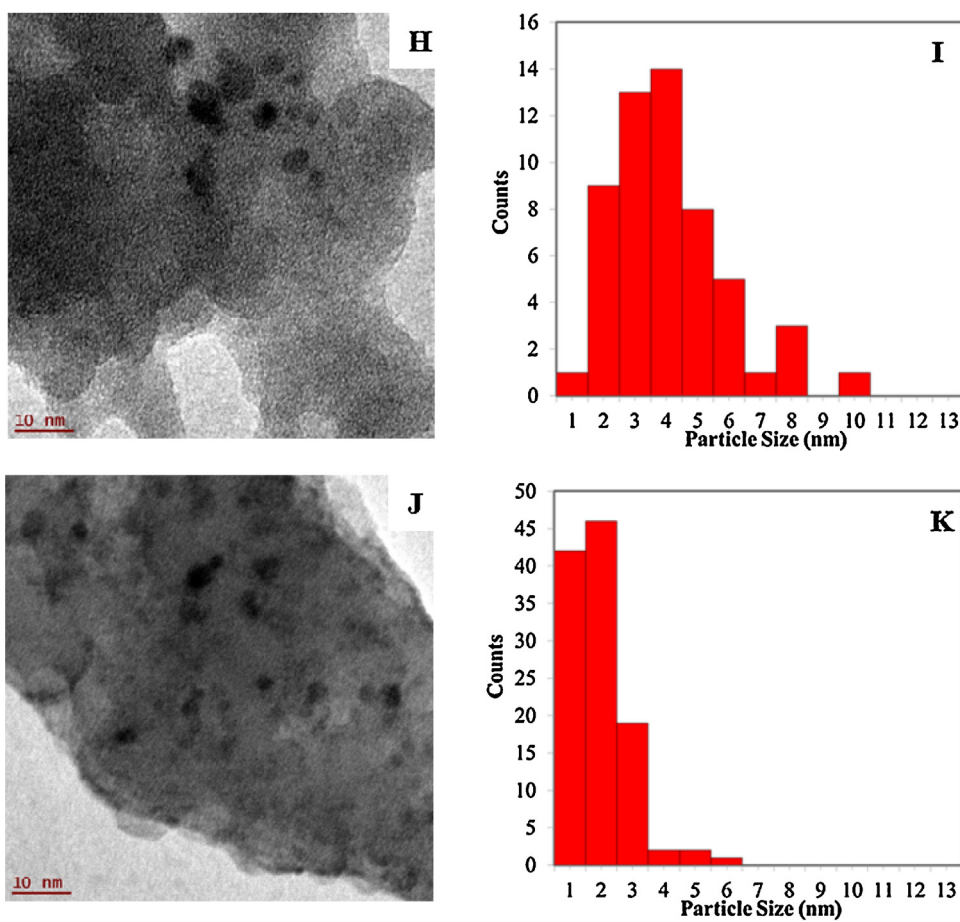
Fig. 3. (*Continued*).

Table 2
Accessible ZrO_2 surface area, ZrO_2 particle size, and surface acid-base properties of Pd catalysts.

Samples	NO_x uptake	ZrO_2 surface area[a]		ZrO_2 particle size (nm)		NH_3 uptake	CO_2 uptake
	(μmol/g)	(m^2/g)	(m^2/g_{ZrO2})	NO_x TPD	XRD	(μmol/g)	(μmol/g)
Fresh Pd/ZrO_2	495	83	84	12	11	111	122
Aged Pd/ZrO_2[b]	148	25	25	41	27	5	10
Fresh Pd/SiO_2	0	0	0	–	–	1	0
Aged Pd/SiO_2[b]	0	0	0	–	–	0	0
Fresh Pd/ZrO_2-SiO_2	327	54	332	3	n.d.	155	2
Aged Pd/ZrO_2-SiO_2[b]	50	8	50	21	n.d.	18	1

[a] Calculated from NO_x TPD experiments.
[b] Aged at 800 °C for 16 h.

in this work (see Table 1) is close to the amount of Zr precursor needed to form a monolayer of ZrO_x in a silanol group to Zr precursor ratio of 2, and that there was an excess Zr precursor in the sol-gel synthesis mixture (see Experimental), it is likely that anchored Zr species underwent major agglomeration during calcination exposing a large fraction of SiO_2 surface. After the aging at 800 °C, NO_x uptake for both catalysts drastically decreased with ZrO_2 surface area of 25 and 8 m^2/g for Pd/ZrO_2 and Pd/ZrO_2-SiO_2, respectively. Note that Pd/ZrO_2 maintained a higher ZrO_2 surface area advantage over Pd/ZrO_2-SiO_2 despite the fact that the latter had a much larger BET surface area. Considering the absence of well crystalline ZrO_2 phases in the XRD patterns (Fig. 2), it is likely that structural changes occurred in SiO_2 during the hydrothermal aging (such as pore blockage) limiting the access to ZrO_2 surfaces. We hypothesize that a higher SiO_2 coverage by ZrO_2 could mitigate the SiO_2 structure evolution, which would in turn minimize loss in accessible ZrO_2 surface area. The ZrO_2 particle sizes estimated from NO_x

uptake are listed in Table 2. The ZrO_2 particle sizes of Pd/ZrO_2 and Pd/ZrO_2-SiO_2 were, respectively, 12 and 3 nm in the fresh state, and 41 and 21 nm after aging at 800 °C. The ZrO_2 particle sizes calculated from NO_x-TPD and XRD (Scherrer equation) were similar for the fresh Pd/ZrO_2, but significantly different for the aged Pd/ZrO_2 possibly due to lattice distortion occurred during the high temperature aging. The absence of ZrO_2-attributable XRD peaks made it impossible to estimate the ZrO_2 crystallite size for the Pd/ZrO_2-SiO_2 catalysts.

It has been reported that high surface acidity and low basicity can confer high sulfur tolerance to a catalytic material [27,28]. The acidic and basic properties of the Pd catalysts studied in the present work were evaluated via temperature programmed desorption of NH_3 and CO_2, respectively. The temperatures of desorption peak maxima (T_m) provide information about the relative strength of acidic or basic sites, while the amount of NH_3 or CO_2 desorbed indicates, respectively, the relative number of acidic or basic sites on
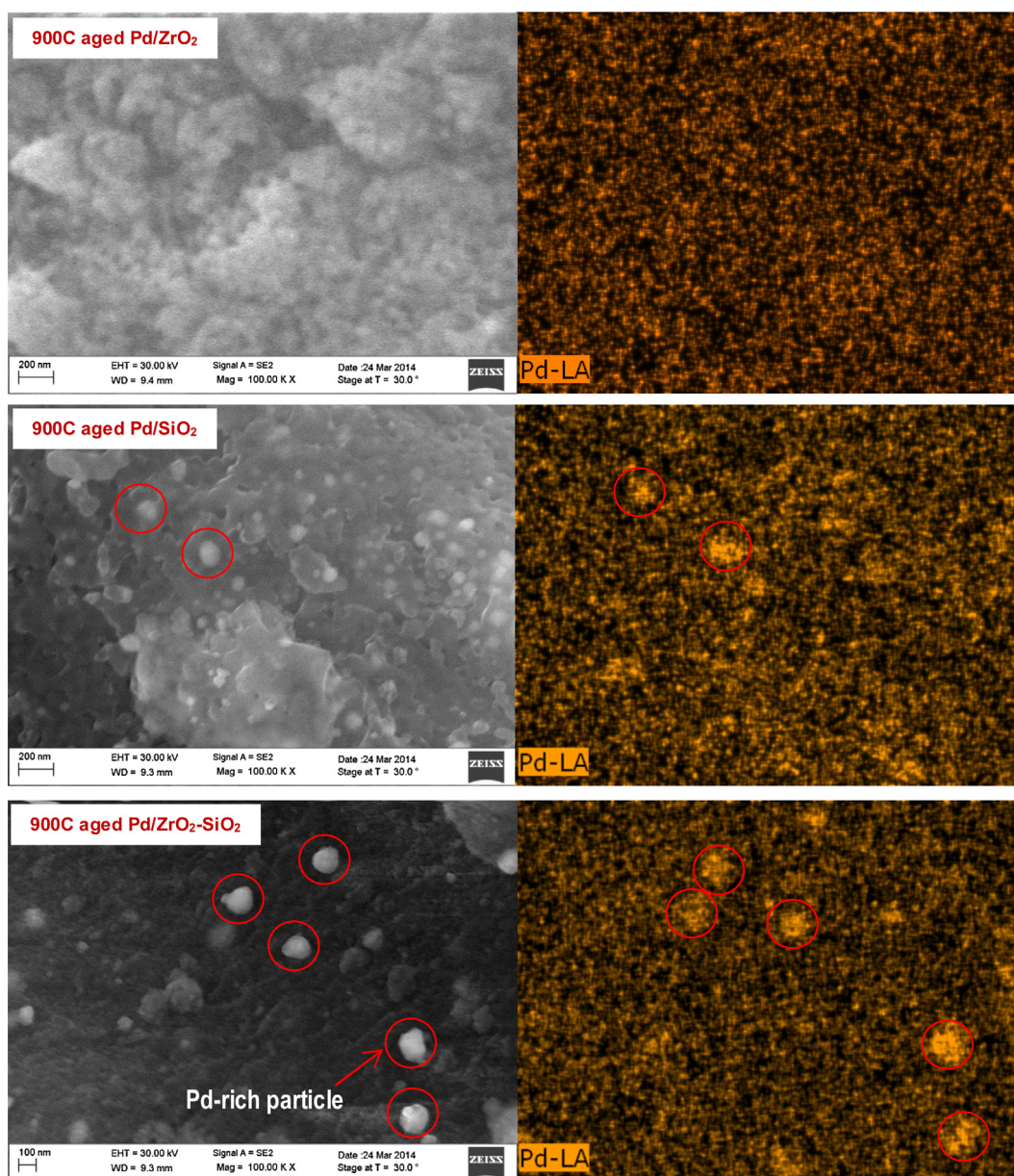
Fig. 4. SEM images (left) and EDX Pd maps (right) of Pd/ZrO$_2$, Pd/SiO$_2$, and Pd/ZrO$_2$-SiO$_2$ in hydrothermally aged state; a few representative Pd-rich particles are marked with circles in the images.

the catalyst surface. As can be seen in Fig. 6, the TPD profile varied significantly with the support type. In the fresh state, Pd/ZrO$_2$ had a large NH$_3$ desorption peak at around 250 °C in contrast to Pd/SiO$_2$ exhibiting negligible NH$_3$ desorption. Pd/ZrO$_2$-SiO$_2$ possessed surface acidity stronger and higher than Pd/ZrO$_2$ as manifested by a larger desorption peak near 270 °C. Based on the NH$_3$-TPD results, the amount and strength of surface acidic sites were estimated to be in the order of Pd/ZrO$_2$-SiO$_2$ > Pd/ZrO$_2$ > Pd/SiO$_2$. This trend agrees well with the previous report that TiO$_2$-SiO$_2$ and ZrO$_2$-SiO$_2$ mixed oxides possess strong acidity [17]. Though most of the catalysts' acidity was lost with aging at 800 °C, Pd/ZrO$_2$-SiO$_2$ still had a relatively higher amount of acid sites (Table 2).

The CO$_2$-TPD experiments showed that Pd/ZrO$_2$ possessed considerable surface basicity also as indicated by a peak at 140 °C in the fresh state (Fig. 6). On the other hand, Pd/SiO$_2$ had no interaction with CO$_2$ confirming its generally inert nature of surface. In the case of Pd/ZrO$_2$-SiO$_2$, CO$_2$ desorption was minor with a small peak at around 130 °C. It is remarkable that ZrO$_2$ deposited on SiO$_2$

presented a surface acido-basicity distinct from that of bulk ZrO$_2$. Conceptually, one could expect that Pd/ZrO$_2$-SiO$_2$ would present a greater sulfur tolerance than Pd/ZrO$_2$, as the former possessed only strong acidity whereas the latter possessed both strong acidity and basicity. As in the case of acidity, the surface basicity of Pd/ZrO$_2$ decreased considerably with aging at 800 °C. Pd/ZrO$_2$-SiO$_2$ presented no CO$_2$ desorption peak after aging. The relative amounts of NH$_3$ and CO$_2$ desorbed are summarized in Table 2. This rather dramatic difference in CO$_2$ uptake between Pd/ZrO$_2$-SiO$_2$ and Pd/ZrO$_2$ suggests that the ZrO$_2$ morphology can play an important role in determining surface acido-basicity of ZrO$_2$-containing catalysts [21,29].

A typical profile of the catalyst outlet sulfur concentration during the sulfation step is shown in Fig. 7 for the Pd/ZrO$_2$ and Pd/ZrO$_2$-SiO$_2$ samples. During the sulfation step, there was an initial short period during which all sulfur was adsorbed, followed by a breakthrough. The total amount of sulfur adsorbed was 14.6 and 13.1 mmol/g$_{cat}$ for Pd/ZrO$_2$ and Pd/ZrO$_2$-SiO$_2$, respectively.
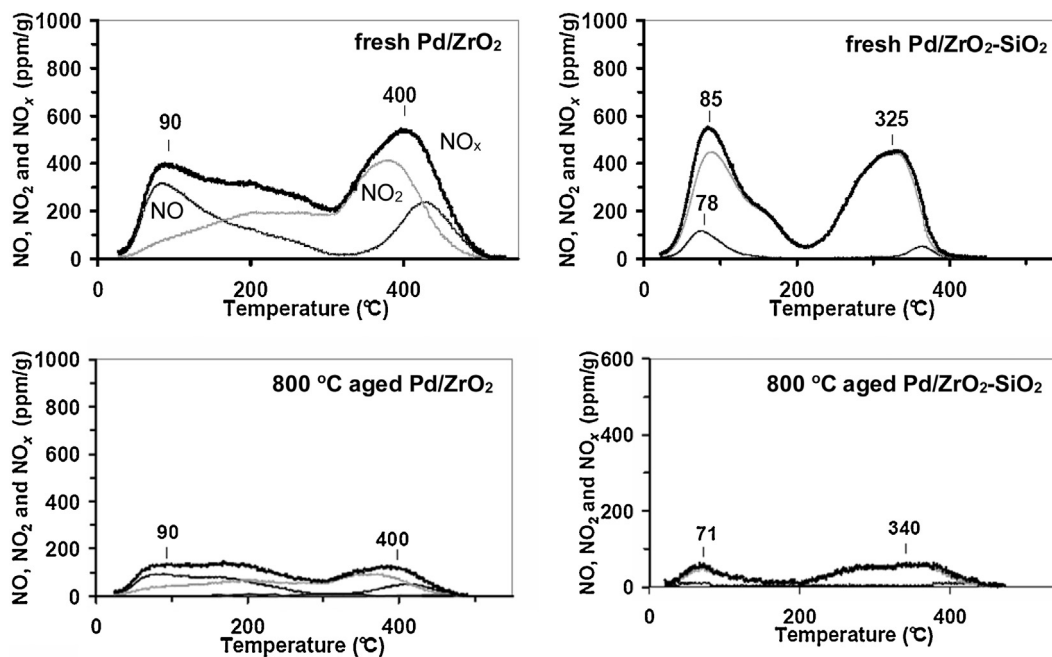
Fig. 5. NO_x-TPD profiles of Pd/ZrO_2 and Pd/ZrO_2-SiO_2 in fresh and hydrothermally aged states.
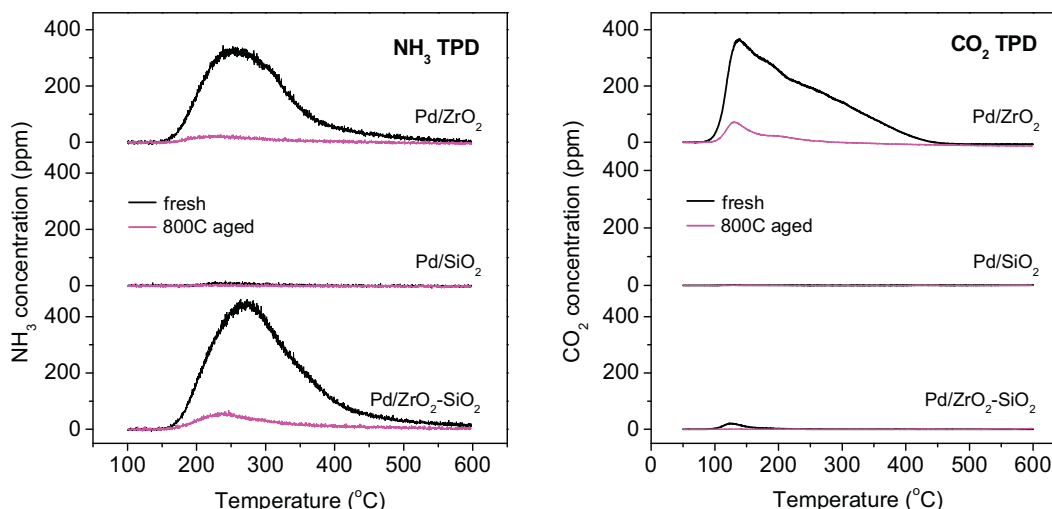

Fig. 6. NH_3 and CO_2 TPD profiles of Pd/ZrO_2, Pd/SiO_2, and Pd/ZrO_2-SiO_2 in fresh and hydrothermally aged states.
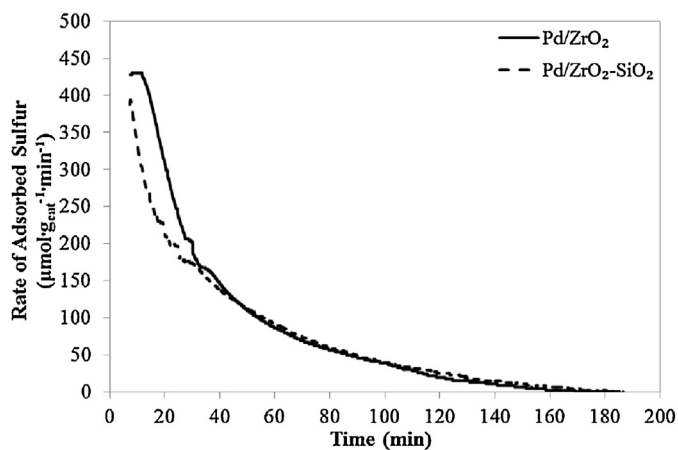

Fig. 7. Rate of SO_2 adsorption measured during the catalyst sulfation (50 ppm SO_2, 5% H_2O, 4% O_2, balance Ar).

This is consistent with the CO_2-TPD experiments which indicated a higher basicity for Pd/ZrO_2. Consecutive temperature-programmed reduction (TPR) runs were performed with the sulfated samples of Pd/ZrO_2 and Pd/ZrO_2-SiO_2 in order to gain further insights into their sulfur affinity. During H_2-TPR, sulfur was released from both catalysts, and the resulting SO_2 release profiles are shown in Fig. 8. For both catalysts, the majority of sulfur was released during the first TPR desulfation (up to 600 °C). For Pd/ZrO_2-SiO_2, the desulfation was almost complete after the second TPR desulfation (up to 700 °C), while the release of sulfur persisted until the third TPR desulfation (up to 800 °C) in the case of Pd/ZrO_2. More specifically, the total amount of desorbed sulfur after desulfation at 800 °C was around 10 and 12 mmol/g_{cat} for Pd/ZrO_2 and Pd/ZrO_2-SiO_2 catalysts, respectively. The discrepancy between the adsorbed and desorbed sulfur was considerable for Pd/ZrO_2 indicating more strongly bound sulfur species remained on the surface. On the other hand, sulfur recovery was almost complete from Pd/ZrO_2-SiO_2 consistent with its low surface basicity leading to more weakly
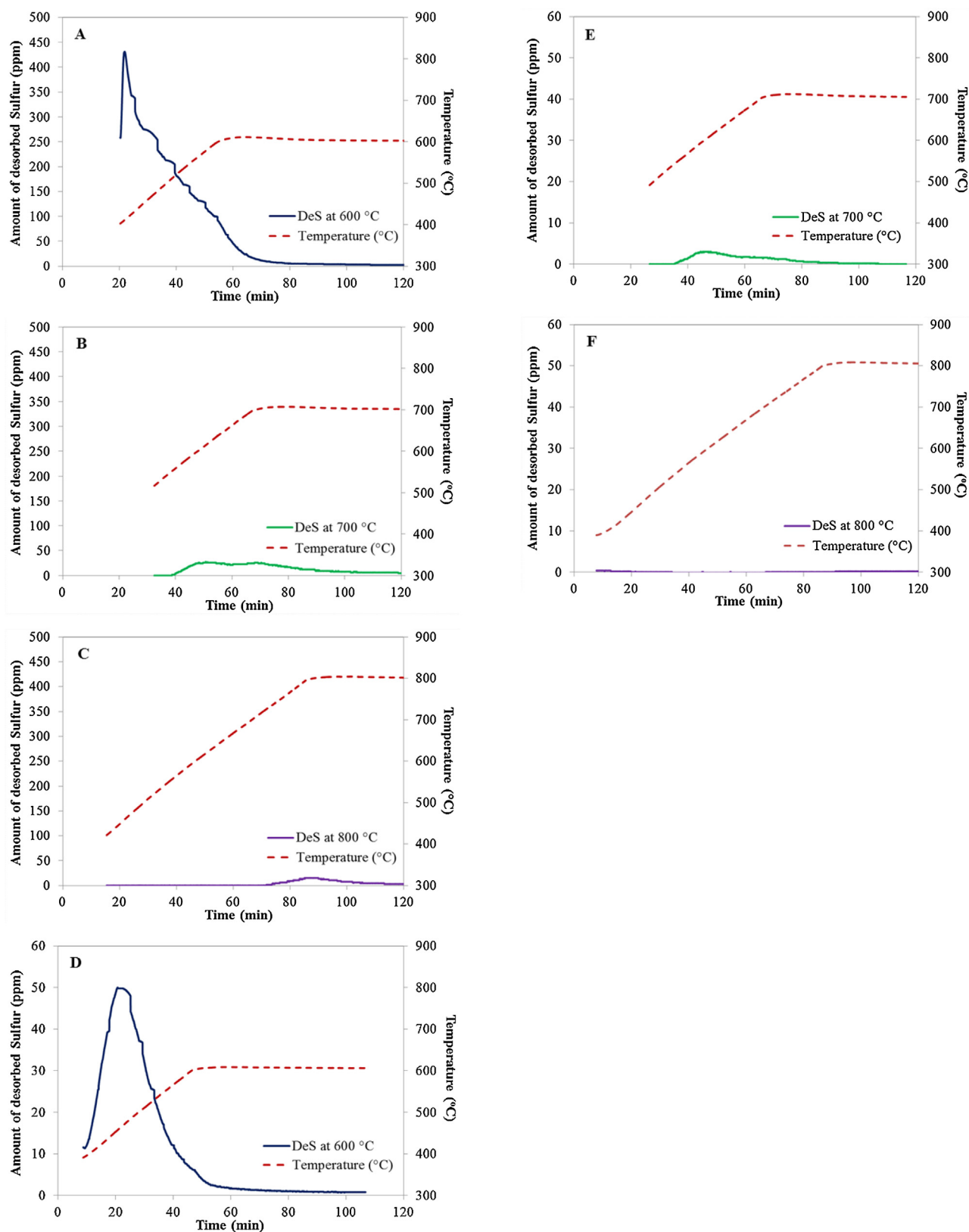
Fig. 8. Sulfur release profiles obtained during consecutive temperature-programmed reduction desulfation runs (1% H_2 and 5% H_2O in Ar; up to 600, 700 and 800 °C) for Pd/ZrO_2 (A-C) and Pd/ZrO_2-SiO_2 (D-F) catalysts.

bound sulfur species. This further emphasizes the importance of controlling ZrO_2 morphology in determining surface acido-basicity and sulfur tolerance of ZrO_2 phases.

3.2. Catalytic performance

Fig. 9 represents the catalytic CO oxidation performance of the Pd catalysts. In addition to the temperature-conversion profiles, the
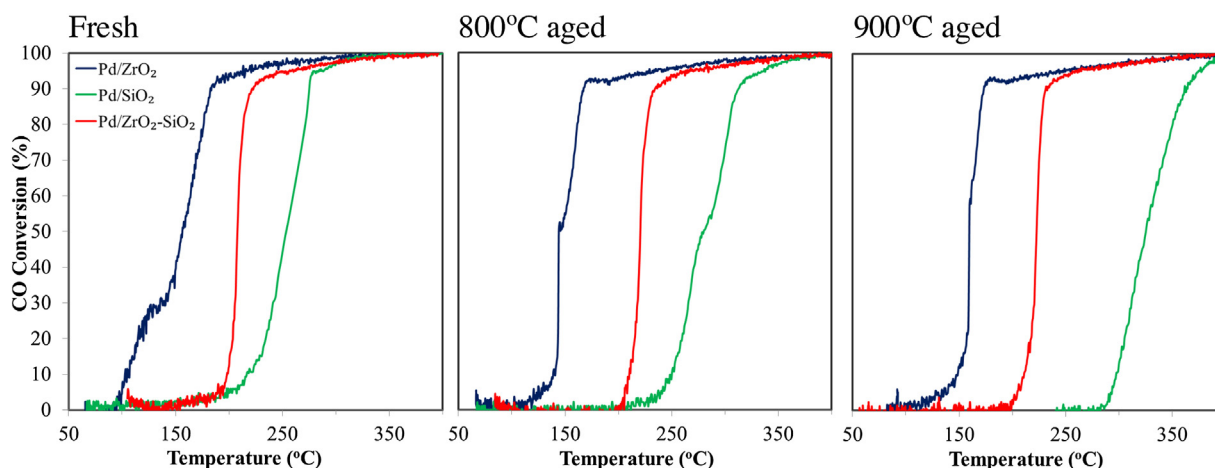
Fig. 9. Catalytic performance of Pd/ZrO_2, Pd/SiO_2, and Pd/ZrO_2-SiO_2 in CO oxidation at a total flow rate of 200 ml/min (4000 ppm CO + 1000 ppm C_3H_6 + 500 ppm NO + 10% O_2 + 5% H_2O + Ar balance) over fresh and hydrothermally-aged catalysts.
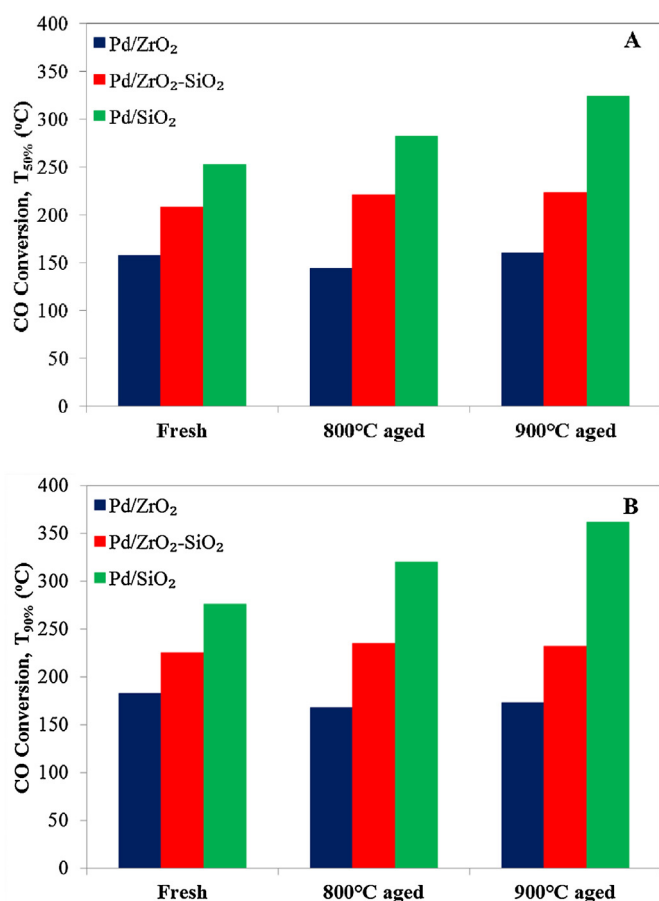

Fig. 10. Comparison of CO conversion $T_{50\%}$ (A) and $T_{90\%}$ (B) for Pd/ZrO_2, Pd/SiO_2 and Pd/ZrO_2-SiO_2 at a total flow rate of 200 ml/min (4000 ppm CO + 1000 ppm C_3H_6 + 500 ppm NO + 10% O_2 + 5% H_2O + Ar balance) over fresh and hydrothermally aged catalysts.

$T_{50\%}$ and $T_{90\%}$ values (the temperatures at which 50% and 90% conversion of CO were achieved, respectively) at different states were determined and summarized in Fig. 10. The fresh Pd catalysts supported on ZrO_2–containing oxides were significantly more active than the fresh Pd/SiO_2. For example, the $T_{90\%}$ for the fresh Pd/ZrO_2 and Pd/ZrO_2-SiO_2 was 183 and 225 °C, respectively, compared to 276 °C for the fresh Pd/SiO_2. Their excellent CO oxidation activity can be attributed to high Pd dispersion due to good metal-support

interaction which could have also affected the electronic state of finely dispersed Pd atoms. The oxidation activity of the Pd/SiO_2 catalysts was significantly decreased after the hydrothermal aging at 800 and 900 °C, while the two ZrO_2-containing catalysts maintained relatively good performance. The stability of Pd/ZrO_2 was especially remarkable with an almost unchanged CO oxidation activity even after 900 °C aging. The fact that both activity loss (Figs. 9, 10) and Pd agglomeration (Figs. 2–4) were significant only with Pd/SiO_2 further highlights the importance of Pd dispersion for oxidation activity.

Fig. 11 presents the catalytic C_3H_6 oxidation performance of the Pd catalysts in fresh, 800 and 900 °C aged states. The $T_{50\%}$ and $T_{90\%}$ values for the C_3H_6 oxidation activity of all the catalysts are listed in Fig. 12. For all catalysts studied, C_3H_6 oxidation light-off occurred at higher temperatures than CO light-off, which is generally observed over other types of catalysts and explained by the fact that C_3H_6 oxidation occurs after CO molecules have been desorbed from the active sites [11,30,31]. Again, Pd/ZrO_2 and Pd/ZrO_2-SiO_2 catalysts exhibited superior C_3H_6 oxidation activity with a $T_{90\%}$ of 192 and 227 °C, respectively. Catalytic performance in C_3H_6 oxidation degraded with hydrothermal aging at 800 and 900 °C, but the ZrO_2-containing catalysts still maintained a good portion of the initial activity compared to Pd/SiO_2.

After sulfation, the CO and C_3H_6 oxidation activity of both catalysts notably decreased and higher temperatures were required for light-off (Figs. 13–16). As an example, the CO oxidation $T_{50\%}$ over Pd/ZrO_2 and Pd/ZrO_2-SiO_2 increased to 226 and 232 °C, respectively (Figs. 13, 15). The performance degradation was greater for the Pd/ZrO_2 catalyst, which can be explained by the larger amount of sulfur being adsorbed on this catalyst (Fig. 7). After desulfation at 600 °C, Pd/ZrO_2-SiO_2 regained its initial activity, whereas 100% of the initial activity could not be fully recovered for the Pd/ZrO_2 catalyst even after desulfation at 800 °C. This is likely due to residual sulfur species on the surface as described above, but the $T_{50\%}$ and $T_{90\%}$ were only 5–10 °C higher for both CO and C_3H_6 (Figs. 15, 16). The desulfation properties were studied under rich conditions in this work, and the results can be relevant to certain diesel applications such as the ones employing lean NO_x traps for NO_x control; as intrinsically cyclic lean/rich operation of lean NO_x traps would allow creating rich exhaust conditions necessary for DOC desulfation placed upstream. However, in lean after treament systems equipped with alternate NO_x control devices for example selective catalytic reduction catalysts, the engine exhausts are expected to be continuously lean. Therefore, further desulfation studies are needed to confirm that ZrO_2–SiO_2 maintains sulfur-
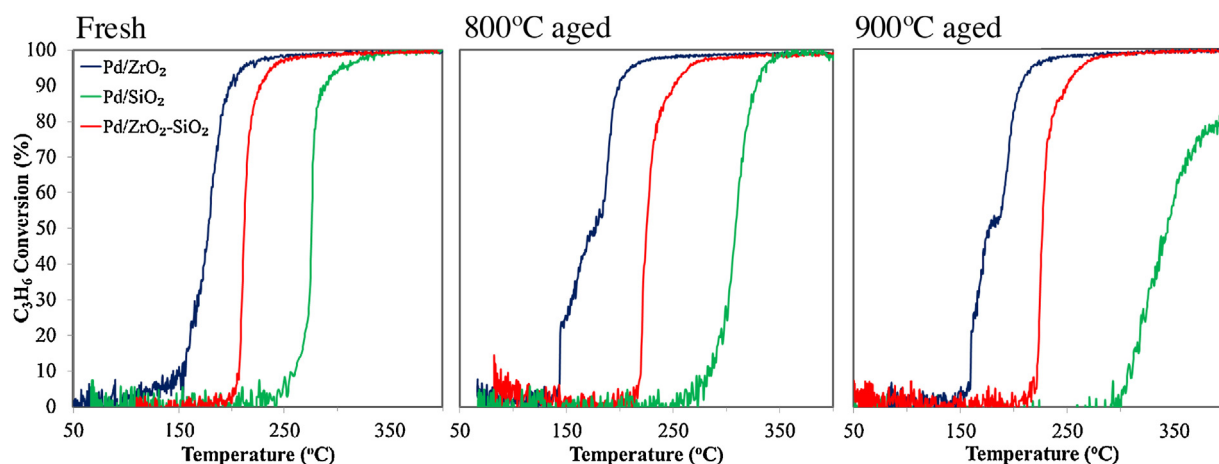
Fig. 11. Catalytic performance of Pd/ZrO_2, Pd/SiO_2, and Pd/ZrO_2-SiO_2 in C_3H_6 oxidation at a total flow rate of 200 ml/min (4000 ppm CO + 1000 ppm C_3H_6 + 500 ppm NO + 10% O_2 + 5% H_2O + Ar balance) over fresh and hydrothermally aged catalysts.
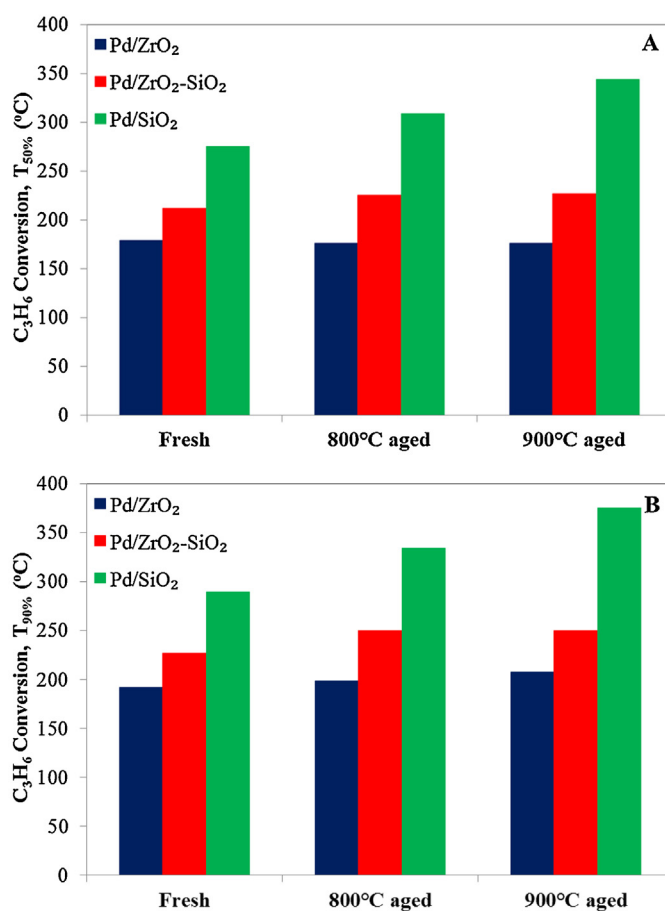

Fig. 12. Comparison of C_3H_6 conversion $T_{50\%}$ (A) and $T_{90\%}$ (B) for Pd/ZrO_2, Pd/SiO_2 and Pd/ZrO_2-SiO_2 at a total flow rate of 200 ml/min (4000 ppm CO + 1000 ppm C_3H_6 + 500 ppm NO + 10% O_2 + 5% H_2O + Ar balance) over fresh and hydrothermally aged catalysts.

tolerance advantage over ZrO_2 in lean desulfation conditions. Our preliminary lean desulfation data reported in Fig. S1 indicate that SO_2 can be removed from Pd/ZrO_2–SiO_2 at significantly lower temperatures than from Pd/ZrO_2.

In summary, the performance data are in good agreement with the characterization results obtained with XRD, TEM, and SEM, which highlight the ability of ZrO_2 to achieve a superior dispersion and stability of Pd particles leading to much better low-temperature CO and C_3H_6 oxidation activity than Pd/SiO_2. In the case of the Pd/ZrO_2-SiO_2 catalyst, as Pd was deposited on both ZrO_2 and SiO_2 surfaces, the oxidation performance was found somewhere between those of Pd/ZrO_2 and Pd/SiO_2 but closer to Pd/ZrO_2. However, the unique ZrO_2 morphology of Pd/ZrO_2-SiO_2 conferred a better sulfur tolerance to this catalyst than Pd/ZrO_2. More complete ZrO_2 coverage of SiO_2 supports or selective deposition of Pd precursors onto ZrO_2 surfaces thus appear to be important design considerations to maximize Pd dispersion and thermal stability potentially leading to a catalyst which outperforms Pd/ZrO_2.
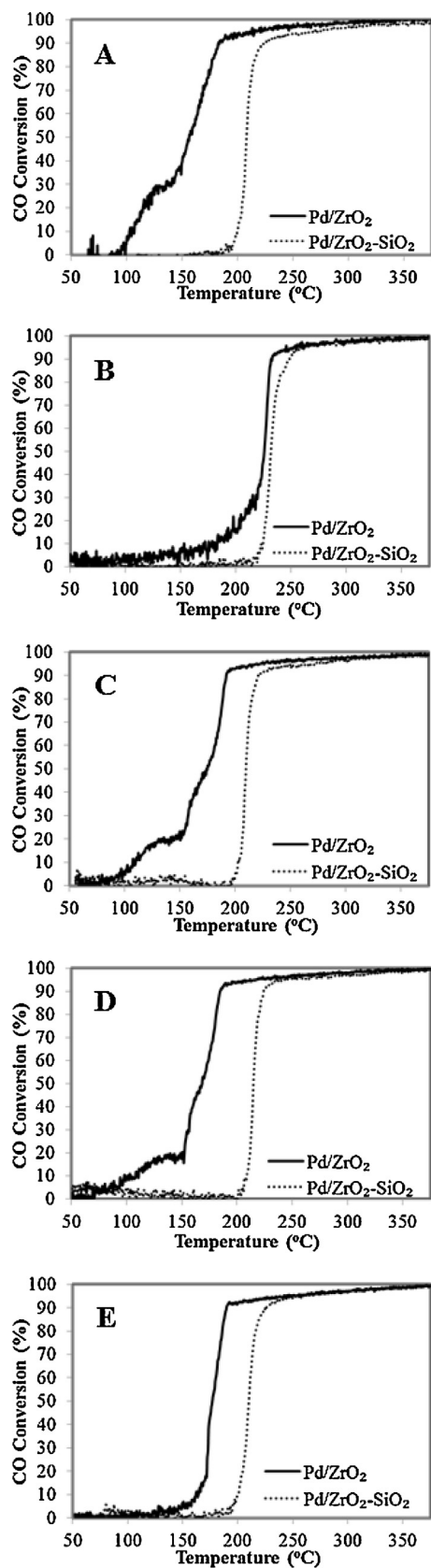
Fig. 13. Catalytic performance of Pd/ZrO_2 and Pd/ZrO_2-SiO_2 in CO oxidation at a total flow rate of 200 ml/min (4000 ppm CO + 1000 ppm C_3H_6 + 500 ppm NO + 10% O_2 + 5% H_2O + Ar balance) over fresh (A), sulfated (B) and desulfated at 600 (C), 700 (D) and 800 °C (E) catalysts.

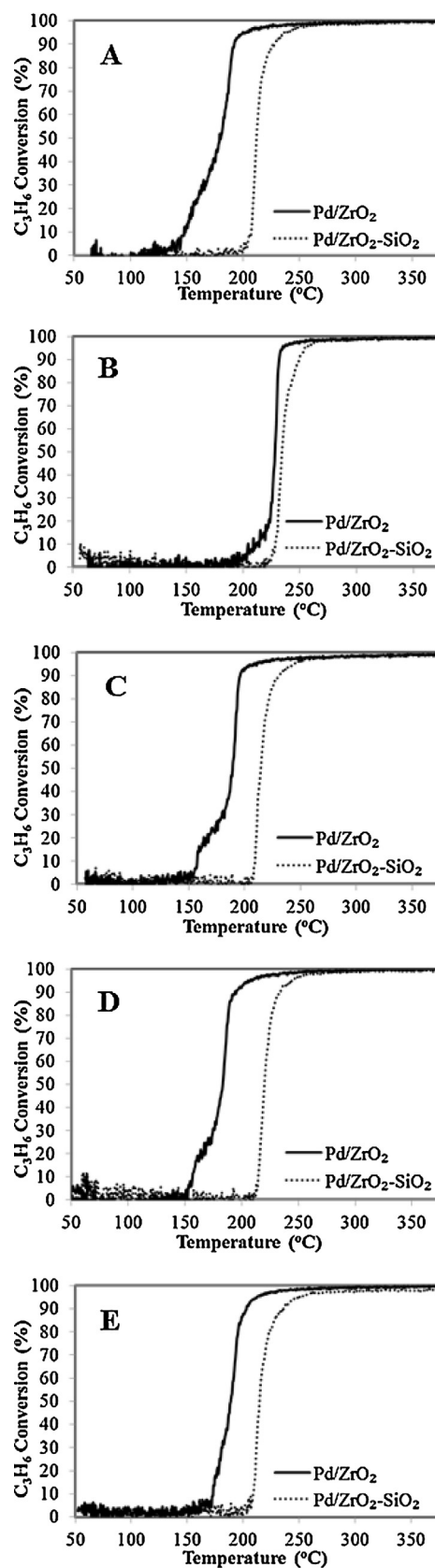**Fig. 14.** Catalytic performance of Pd/ZrO_2, Pd/SiO_2, and Pd/ZrO_2-SiO_2 in C_3H_6 oxidation at a total flow rate of 200 ml/min (4000 ppm CO + 1000 ppm C_3H_6 + 500 ppm NO + 10% O_2 + 5% H_2O + Ar balance) over fresh (A), sulfated (B) and desulfated at 600 (C), 700 (D) and 800 °C (E) catalysts.
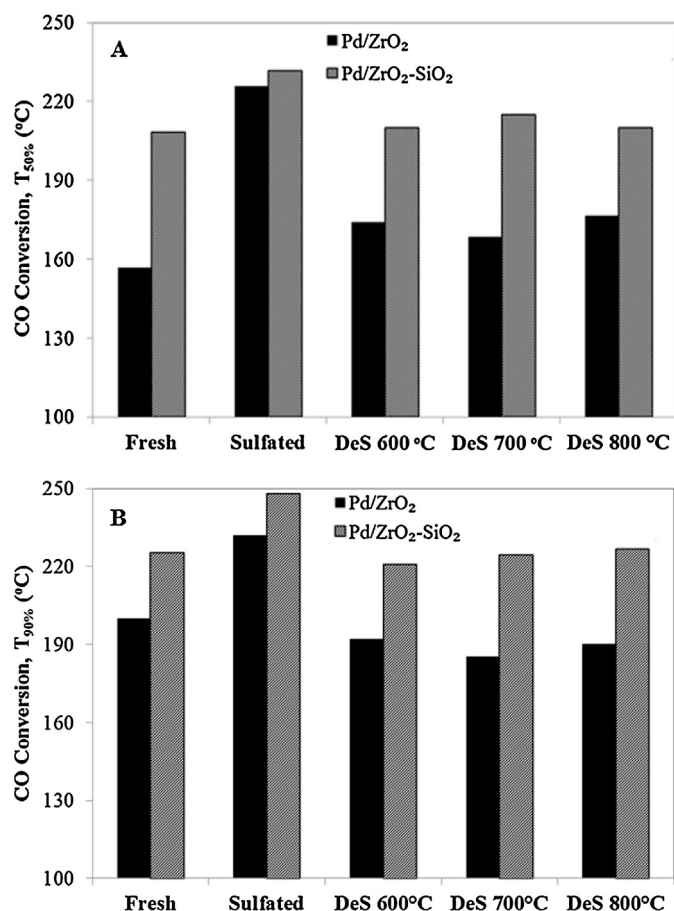
Fig. 15. Comparison of CO conversion $T_{50\%}$ (A) and $T_{90\%}$ (B) for Pd/ZrO$_2$ and Pd/ZrO$_2$-SiO$_2$ catalysts at fresh, sulfated and desulfated (DeS) at various temperatures states at a total flow rate of 200 ml/min (4000 ppm CO + 1000 ppm C$_3$H$_6$ + 500 ppm NO + 10% O$_2$ + 5% H$_2$O + Ar balance).

Fig. 16. Comparison of C$_3$H$_6$ conversion $T_{50\%}$ (A) and $T_{90\%}$ (B) for Pd/ZrO$_2$ and Pd/ZrO$_2$-SiO$_2$ catalysts at fresh, sulfated and desulfated (DeS) at various temperatures states at a total flow rate of 200 ml/min (4000 ppm CO + 1000 ppm C$_3$H$_6$ + 500 ppm NO + 10% O$_2$ + 5% H$_2$O + Ar balance).

4. Conclusions

We investigated the impact of ZrO$_2$ on the catalytic performance of Pd-based oxidation catalysts in simulated lean automotive exhaust conditions. Key findings in the present study were:

- ZrO$_2$ is an excellent support for Pd catalysts leading to high dispersion, hydrothermal stability, and low-temperature CO and C$_3$H$_6$ oxidation activity;
- ZrO$_2$ incorporation on SiO$_2$ via sol-gel method before Pd impregnation led to enhanced dispersion and hydrothermal stability of Pd due to stronger interaction between Pd and supports;
- Likely due to its unique morphology, the ZrO$_2$ phases incorporated on SiO$_2$ surface presented strong acidity but negligible strong basicity on the surface, whereas bulk ZrO$_2$ had both strong acidity and basicity;
- Lack of strong basicity imparted an excellent sulfur tolerance to Pd/ZrO$_2$-SiO$_2$;
- Incomplete coverage of SiO$_2$ surface by ZrO$_2$ led to an overall lower accessible ZrO$_2$ surface area and Pd deposition on both ZrO$_2$ and SiO$_2$ surfaces limiting the full potential of Pd/ZrO$_2$-SiO$_2$ catalyst concept in the samples evaluated here;
- Further research is necessary to further our understanding of the structure and chemistry of ZrO$_2$ layer on SiO$_2$ and to find strategies to obtain more complete ZrO$_2$ coverage of SiO$_2$ and selective Pd deposition on ZrO$_2$ surfaces.
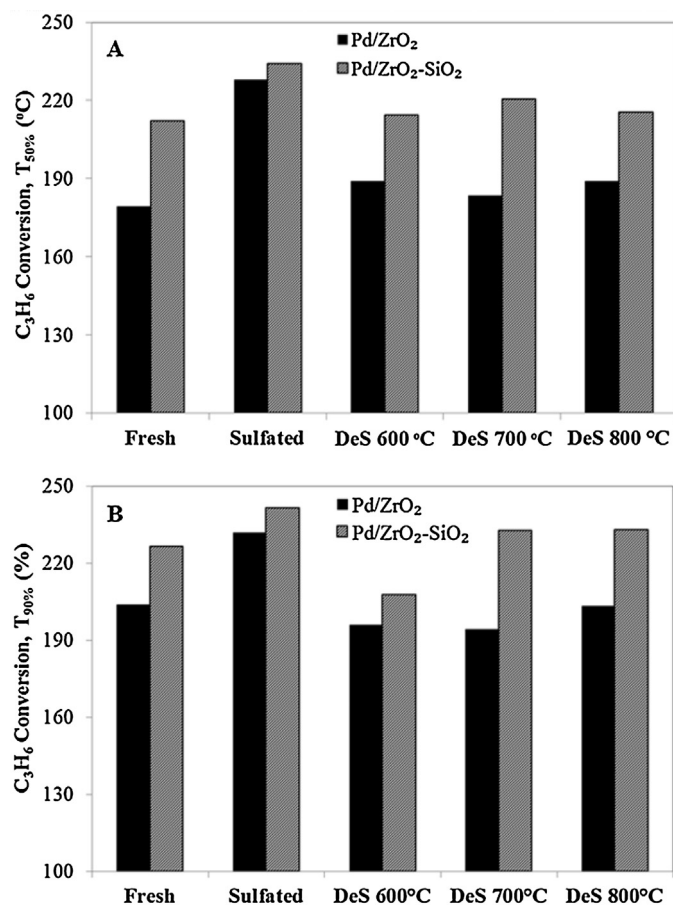
Appendix A. Supplementary data

Supplementary data associated with this article can be found, in the online version, at http://dx.doi.org/10.1016/j.apcatb.2016.01.023.

References

[1] A. Russell, W.S. Epling, Catal. Rev. Sci. Eng. 53 (2011) 337.
[2] T.V. Johnson, SAE Int. J. Fuels Lubr. 2 (2009) 1.
[3] A. Manigrasso, N. Fouchal, P. Darcy, P.D. Costa, Catal. Today 191 (2012) 52.
[4] M. Haruta, J. New. Mat. Electrochem. Syst. 7 (2004) 163.
[5] L. Li, Q. Chen, Q. Zhang, J. Shi, Y. Li, W. Zhao, J. Shi, Catal. Commun. 26 (2012) 15.
[6] S. Li, H. Zhu, Z. Qin, G. Wang, Y. Zhang, Z. Wu, Z. Li, G. Chen, W. Dong, Z. Wu, L. Zheng, J. Zhang, T. Hu, J. Wang, Appl. Catal. B: Environ. 144 (2014) 498.
[7] X. Zhang, Z. Qu, F. Yu, Y. Wang, J. Catal. 297 (2013) 264.
[8] S. Golunski, Platinum Metals Rev. 51 (2007) 162.
[9] J.A. Moulijn, A.E. Diepen, F. Kapteijn, Appl. Catal. A: Gen. 212 (2001) 3.
[10] H. Shinjoh, Catal. Surv. Asia 13 (2009) 184.

[11] F.C. Galisteo, R. Mariscal, M.L. Granados, M.D.Z.A. Poves, J.L.G. Fierro, V. Kröger, R.L. Keiski, Appl. Catal. B: Environ. 72 (2007) 272.
[12] L. Liu, F. Zhou, L. Wang, Z. Qi, F. Shi, Y. Deng, J. Catal. 274 (2010) 1.
[13] A. Tomita, K. Shimizu, K. Kato, Y. Tai, Catal. Commun. 17 (2012) 194.
[14] Y. Shen, G. Lu, Y. Guo, Y. Wang, Y. Guo, L. Wang, X. Zhen, Catal. Commun. 18 (2012) 26.
[15] M. Cargnello, J.J.D. Jaén, J.C.H. Garrido, K. Bakhmutsky, T. Montini, J.J.G. Gámez, R.J. Gorte, P. Fornasiero, Science 337 (2012) 713.
[16] X. Guo, Q. Fu, Y. Ning, M. Wei, M. Li, S. Zhang, Z. Jiang, X. Bao, J. Am. Chem. Soc. 134 (2012) 12350.
[17] M.-Y. Kim, J.-S. Choi, T. Toops, E.-S. Jeong, S.-W. Han, V. Schwartz, Catalysts 3 (2013) 88.
[18] M.-Y. Kim, S.M. Park, G. Seo, K.-S. Song, Catal. Lett. 138 (2010) 205.
[19] B. Buszewski, S. Bocian, G. Rychlicki, M. Matyska, J. Pesek, J. Chromatogr. A 1232 (2012) 43.
[20] C. Thomas, J. Phys. Chem. C 115 (2011) 2253.
[21] H.Y. Law, J. Blanchard, X. Carrier, C. Thomas, J. Phys. Chem. C 114 (2010) 9731.
[22] T.J. Toops, B.G. Bunting, K. Nguyen, A. Gopinath, Catal. Today 123 (2007) 285.
[23] T.J. Toops, N.A. Ottinger, C. Liang, J.A. Pihl, E.A. Payzant, Catal. Today 160 (2011) 131.
[24] Z.A. Alothman, Materials 5 (2012) 2874.
[25] S. Jayakumara, P.V. Ananthapadmanabhan, K. Perumal, T.K. Thiyagarajan, S.C. Mishra, L.T. Sue, A.I.Y. Toke, J. Guo, Mater. Sci. Eng. B 176 (2011) 894.
[26] T. Bonnotte, C. Sayag, R.P. Doherty, J.-M. Krafft, C. Méthivier, F. Ser, M. Sicard, C. Thomas, J. Phys. Chem. C 118 (2014) 7386.
[27] J. Oi-Uchisawa, A. Obuchi, R. Enomoto, S. Liu, T. Nanba, S. Kushiyama, Appl. Catal. B 26 (2000) 17.
[28] S. Matsumoto, Y. Ikeda, H. Suzuki, M. Ogai, N. Miyoshi, Appl. Catal. B 25 (2000) 115.
[29] K. Pokrovski, K. Taek Jung, A.T. Bell, Langmuir 17 (2001) 4297.
[30] C. Larese, M.L. Granados, F.C. Galisteo, R. Mariscal, J.L.G. Fierro, Appl. Catal. B: Environ. 62 (2006) 132.
[31] J.M.A. Harmsen, J.H.B.J. Hoebink, J.C. Shouten, Ind. Eng. Chem. Res. 39 (2000) 599.